

# Ground- and Excited-State Electronic Structures of the Solar Cell Sensitizer Bis(4,4'-dicarboxylato-2,2'-bipyridine)bis(isothiocyanato)ruthenium(II)

Jeremy E. Monat,<sup>†,‡</sup> Jorge H. Rodriguez,<sup>§</sup> and James K. McCusker<sup>\*,†,‡</sup>

Department of Chemistry, University of California at Berkeley, Berkeley, California 94720-1460,  
Department of Chemistry, Michigan State University, East Lansing, Michigan 48824-1322, and  
Department of Physics, Purdue University, West Lafayette, Indiana 47907-1396

Received: April 8, 2002; In Final Form: June 10, 2002

The ground- and excited-state electronic structures of the photosensitizer bis(4,4'-dicarboxylato-2,2'-bipyridine)-bis(isothiocyanato)ruthenium(II),  $[\text{RuL}'_2(\text{NCS})_2]^{4-}$  (where  $\text{L}' = 4,4'$ -dicarboxylato-2,2'-bipyridine), have been examined computationally in an effort to better understand this molecule's effectiveness in  $\text{TiO}_2$ -based photoelectrochemical cells. Density functional theory (DFT) calculations of the compound's ground state indicate that occupied molecular orbitals (MOs) localized on carboxylate groups of the bipyridyl ligands (through which the compound binds to the  $\text{TiO}_2$  nanoparticles) energetically match the semiconductor valence band; the lowest unoccupied MOs lie above the conduction band edge and are bipyridine  $\pi^*$  in character. These results suggest that the compound is well-positioned to bind strongly to  $\text{TiO}_2$  and engage in electron transfer from excited states associated with the bipyridyl groups. Various excited states of the chromophore were identified using time-dependent density functional theory (TD-DFT). The TD-DFT calculations predict with significant accuracy excitation energies and corresponding oscillator strengths of transitions observed in the experimental electronic absorption spectrum in ethanol solution. Some of the calculated singlet excited states show significant electronic localization on the bipyridyl groups which, in conjunction with their energies and relatively large oscillator strengths, suggests that these states can be involved in efficient excited-state formation and subsequent electron injection into the  $\text{TiO}_2$  conduction band. Considering both oscillator strength and spatial proximity, the most efficient electronic injection is expected at excitation energies of approximately 2.3, 3.0, and 3.2 eV. Finally, some implications of these results for the molecular engineering of solar cell sensitizers are discussed.

## Introduction

Dye-sensitized solar energy cells have received considerable attention over the past decade.<sup>1–5</sup> From a chemical point of view, these devices are interesting because the light-absorbing sensitizer may be engineered independent of the electron-transporting semiconductor to improve energy conversion efficiency. For a compound to be an effective sensitizer, it must meet several requirements. First, it should adsorb strongly to the semiconductor via anchoring groups<sup>6</sup> to ensure device stability and good electronic coupling for charge injection. Second, its absorption cross-section should match the solar spectrum to form excited states capable of injection into the semiconductor's conduction band.<sup>3</sup> Finally, following injection, the kinetic re-reduction of the now-oxidized chromophore should be rapid enough to prevent charge recombination with electrons in the conduction band, a process that diminishes photocurrents. A major factor in determining whether a dye can fulfill these requirements is its electronic structure. Previous experimental work has examined sensitizer energetics,<sup>2</sup> device kinetics,<sup>7–27</sup> etc., and their interplay; however, more detailed information about the electronic structures of the chromophores being employed would be helpful in designing improved sensitizers.

To consider a specific example, bis(4,4'-dicarboxylic acid-2,2'-bipyridine)bis(isothiocyanato)ruthenium(II)/ $\text{TiO}_2$ , or  $\text{Ru}(\text{H}_2\text{L}')_2(\text{NCS})_2/\text{TiO}_2$ , comprises a solar energy cell with 5–10% efficiency<sup>5</sup> and has been widely investigated. While its similarity to  $[\text{Ru}(\text{bpy})_3]^{2+}$  ( $\text{bpy} = 2,2'$ -bipyridine) makes that widely known complex a reasonable starting point for understanding of the electronic properties of  $\text{Ru}(\text{H}_2\text{L}')_2(\text{NCS})_2$ , the reduced symmetry, redox-tuning isothiocyanate ligands, and presence of carboxy groups on the bipyridines make  $\text{Ru}(\text{H}_2\text{L}')_2(\text{NCS})_2$  itself worth studying. Various aspects of this compound's electronic structure have been previously investigated. Rensmo et al. determined the energy of the dye's highest occupied molecular orbital (HOMO) relative to that of the valence band of  $\text{TiO}_2$  using photoelectron spectroscopy.<sup>28</sup> These authors then used semiempirical calculations to find the relative energies and atomic compositions of various MOs and simulated the photoelectron spectrum. The electronic absorption spectrum of the related complex  $\text{Ru}(\text{bpy})_2(\text{NCS})_2$  has also been simulated with fairly good accuracy (average absolute error of two visible peaks  $\sim 0.21$  eV).<sup>29</sup> To determine the relative energetics of the dye excited state and the  $\text{TiO}_2$  conduction band, Moser et al. used the flatband potential of  $\text{TiO}_2$  ( $\sim -0.8$  V vs SCE) and the oxidation potential of  $\text{Ru}(\text{H}_2\text{L}')_2(\text{NCS})_2$  (+0.86 V vs SCE)<sup>30</sup> along with the 0–0 excitation energy of  $\text{Ru}(\text{H}_2\text{L}')_2(\text{NCS})_2$  (1.75 eV) into its lowest-energy electronic absorption band.<sup>2</sup> These authors concluded that even the lowest-energy <sup>1</sup>MLCT excited state has enough energy to inject into  $\text{TiO}_2$ .<sup>30</sup> This is consistent

\* Author to whom correspondence should be addressed at Department of Chemistry, Michigan State University, 320 Chemistry Building, East Lansing, MI 48824-1322.

<sup>†</sup> Michigan State University.

<sup>‡</sup> University of California at Berkeley.

<sup>§</sup> Purdue University.

with the experimental observation that the injection quantum yield is essentially independent of excitation wavelength out to  $\sim 670$  nm (1.85 eV).<sup>30</sup> While excited triplet states (e.g., <sup>3</sup>MLCT) are not expected to contribute substantially to the ground-state absorption cross-section of this sensitizer, they could still play an important role in the injection dynamics following intersystem crossing from the initially formed singlets. Indeed, triplet excited states have been implicated in electron injection from this sensitizer<sup>31,27</sup> (and others<sup>32,33,25</sup>) based on the analysis of ultrafast transient absorption data, though the triplet zero-point energies have not been determined.

While previous semiempirical studies yielded important information, the aforementioned issues could be further understood by electronic structure calculations that incorporate to a higher degree the effects of electron correlation.<sup>34</sup> A comprehensive theoretical method to study the ground- and excited-state electronic structure of transition metal complexes, which are the most common sensitizers, has recently become available. It begins with a density functional theory (DFT) analysis, which provides information about the ground-state electronic structure. Next, time-dependent density functional theory (TD-DFT) is used to find the characters, energies, and oscillator strengths of singlet and triplet excited states. We have applied this DFT-based method to the quadruply deprotonated form of  $\text{Ru}(\text{H}_2\text{L}')_2(\text{NCS})_2$ , which we will refer to as  $[\text{RuL}'_2(\text{NCS})_2]^{4-}$  (bis(4,4'-dicarboxylato-2,2'-bipyridine)bis(isothiocyanato)-ruthenium(II)), to elucidate its ground- and excited-state electronic structures. We have used these calculations to simulate the electronic absorption spectrum of the complex. These results provide insights into the origins of the observed transitions as well as their possible role in dye-sensitized solar cell injection dynamics.

## Experimental Section

**Computational Methods.** The geometry of  $[\text{RuL}'_2(\text{NCS})_2]^{4-}$  used for the calculations corresponds to the single-crystal X-ray structure reported by Shklover et al.<sup>35</sup> The unprotonated state was chosen because it is the predominant form in neutral solvents such as 5:1 water/ethanol.<sup>36</sup> Furthermore, its electronic absorption spectrum is not noticeably different whether the complex is dissolved in ethanol or adsorbed to the  $\text{TiO}_2$  photoelectrode<sup>31</sup> and the fully deprotonated form performs fairly well as a solar cell sensitizer.<sup>36</sup> All calculations were performed with Gaussian 98<sup>37</sup> using a spin-restricted formalism at the B3LYP/LanL2DZ level of theory which has proven useful for other ruthenium polypyridyl complexes.<sup>38</sup> No geometry optimization was performed because this method tends to overestimate metal–ligand bond lengths with basis sets that, due to the large size of the molecule, are modest and far from the basis set limit;<sup>39</sup> no symmetry was imposed. Effective core potentials were used for the ruthenium and sulfur atoms only; all other atoms were treated with their full complement of electrons. TD-DFT excited-state calculations were performed based on the B3LYP/LanL2DZ ground-state reference.

**Electronic Absorption Spectrum.**  $\text{Ru}(\text{H}_2\text{L}')_2(\text{NCS})_2$  was purchased from Solaronix (Lausanne, Switzerland). Absolute ethanol was distilled over 4 Å molecular sieves immediately prior to use. Spectra were recorded on a Hewlett-Packard 8452A spectrophotometer.

## Results and Discussion

With regard to solar cell performance, three aspects of the sensitizer's electronic structure can be considered: (1) the energetic overlap between the semiconductor valence band and

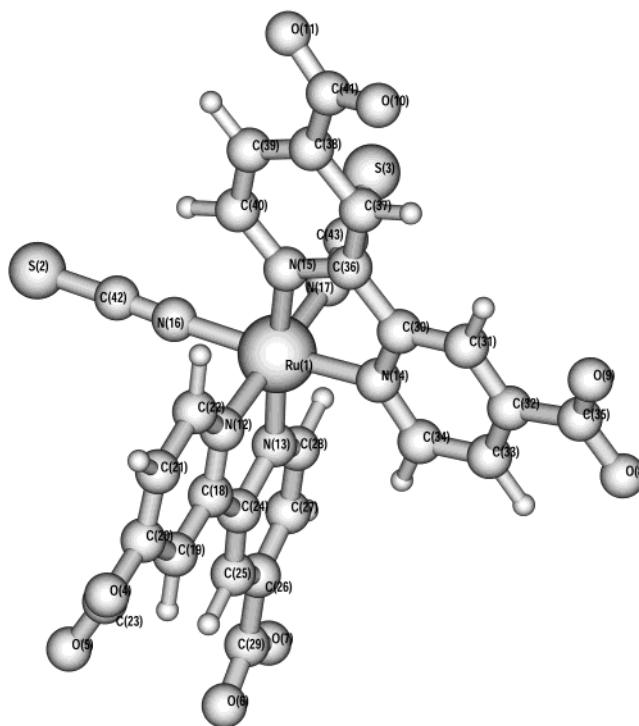


**Figure 1.** Drawing of the complex  $[\text{RuL}'_2(\text{NCS})_2]^{4-}$  obtained from the X-ray structure determination by Shklover et al.<sup>35</sup>

dye molecular orbitals centered near the anchoring points to promote chemisorption to the semiconductor surface; (2) charge localization of excited states near the anchoring points to facilitate the electronic coupling necessary for charge injection; and (3) the energetics of these excited states relative to the conduction band of the semiconductor to provide a thermodynamic driving force for injection. These issues can all be addressed through an examination of the molecule's ground and excited states.

**Ground-State Electronic Structure.** The experimental geometry<sup>35</sup> for  $[\text{RuL}'_2(\text{NCS})_2]^{4-}$  is shown in Figure 1. Although the complex has a  $\text{N}_6$  coordination environment, the local symmetry is far from octahedral because of the two different ligands (i.e., 4,4'-dicarboxylato-2,2'-bipyridine and isothiocyanate). Further, the approximate  $C_2$  symmetry<sup>35</sup> is broken due to differing orientations of the carboxylate groups, reducing the overall molecular point group to  $C_1$ .

The ground-state electronic structure was calculated in order to determine the energies and compositions of the MOs. The frontier orbitals are plotted according to their energies in Figure 2. The assignment of the type of each MO was made on the basis of its composition (Table 1) and by visual inspection of its three-dimensional representation (e.g., Figure 3). Some lower-energy occupied MOs are centered on the carboxylate groups and the isothiocyanate ligands. The two highest occupied MOs (152 and 153) are mainly ruthenium d-orbital in character, but are antibonding with respect to the isothiocyanate ligands as shown by the appreciable electron density on the nitrogen and sulfur atoms (Table 1 and Figure 3). This is consistent with the report of Rensmo et al., who determined that the HOMOs were largely of ruthenium d-orbital origin, yet had significant density on the isothiocyanate ligands.<sup>28</sup> Our results are also in agreement with the DFT study of  $[\text{Ru}(\text{bpy})_3]^{2+}$  by Daul et al.<sup>40</sup> wherein the highest occupied MOs were mainly of metal character and were  $\pi$  antibonding, with the caveat that for  $[\text{RuL}'_2(\text{NCS})_2]^{4-}$  it is the isothiocyanate ligands, rather than bipyridines, to which the metal is  $\pi$  antibonding (Figure 3). In our calculations,

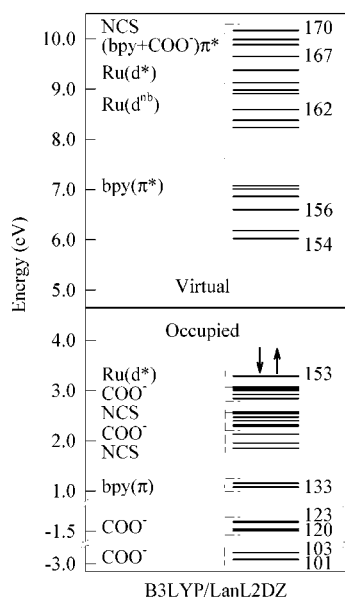


**Figure 2.** Energy level diagram of  $[\text{RuL}'_2(\text{NCS})_2]^{4-}$  frontier molecular orbitals calculated at the B3LYP/LanL2DZ level. Labels on the left denote the dominant moiety contributing to each molecular orbital (nb: nonbonding; \*: antibonding). For clarity, only a few of the molecular orbitals are numbered.

LUMO and seven subsequent virtual (unoccupied) orbitals are essentially  $\pi^*$  orbitals of the bipyridine moieties (e.g., Figure 3a). These lowest eight unoccupied MOs show little localization on the carboxylate groups. The three other ruthenium orbitals with mainly d character are still higher in energy and display nonbonding (MO 162: 8.589 eV; MO 163: 8.909 eV; MO 164: 8.976 eV) or antibonding (MO 165: 9.125 eV; MO 166: 9.374 eV; MO 167: 9.645 eV) interactions with the ligands.

As a result of the lack of symmetry in this complex, the ground-state electronic structure contains little degeneracy. For example, the metal-rich MOs 152 and 153 have a fairly large energy splitting of 0.208 eV. This is partly because the relevant d orbital is destabilized by antibonding interactions with two isothiocyanates in MO 153, but only one isothiocyanate in MO 152 (Figure 3b). Another consequence of the highly distorted octahedral symmetry is that there are only two occupied ruthenium d orbitals, as opposed to the three for a typical ruthenium octahedral complex. This indicates that ruthenium has a significantly different interaction with the isothiocyanate ligands than with the bipyridine, which is reasonable given their relative positions in the spectrochemical series.

Frontier orbitals are described more quantitatively in Table 1. From the energies listed, we note that there is a HOMO–LUMO gap of 2.736 eV. The percent composition of each MO is also listed for noteworthy atoms. It is interesting to examine the correlation between energy and degree of delocalization for related MOs. For example, while all four virtual orbitals listed are bipyridine  $\pi^*$  in character, MOs 154–155 are spread over both halves of a given bipyridine moiety, while MOs 156–157 are primarily localized to a single pyridine within a bipyridine moiety (Figure 3a).

MOs which are likely involved in bonding to the semiconductor are those localized on the anchoring carboxylate moieties of the dicarboxybipyridine ligands. Carboxylate-based MOs 101–103 and 120–123 are, in fact, within the  $\text{TiO}_2$  valence band energy range.<sup>28</sup> Taken together, these MOs have significant electron localization on all four carboxylate moieties, suggesting that any of the four could contribute to adsorption to the semiconductor. It follows that strong adsorption would be

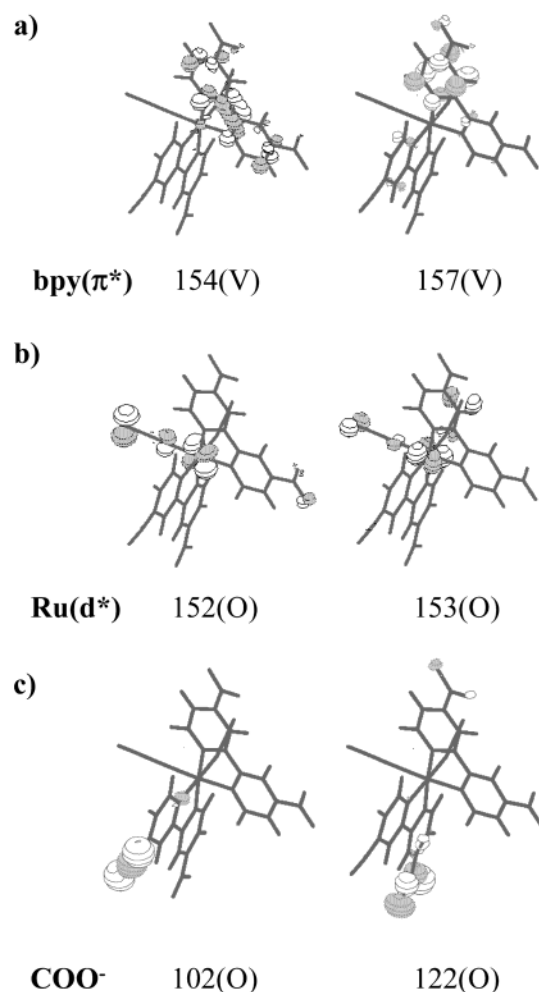


**Figure 3.** Selected molecular orbitals of  $[\text{RuL}'_2(\text{NCS})_2]^{4-}$ . (a) Bipyridine-based  $\pi^*$  virtual (V) MOs 154 and 157. (b) Occupied (O) ruthenium-based  $d^*$  MOs 152 and 153. (c) Occupied (O) carboxylate-based MOs 102 and 122.

facilitated by a sensitizer– $\text{TiO}_2$  arrangement which maximizes the number of bound carboxylates.

A simple Mulliken charge analysis of the ground-state wave function gives the ruthenium ion charge as +1.051, well below its formal value of +2 in a simple ionic view. This indicates significant covalency in the metal–ligand interactions.

**Time-Dependent Calculations of Singlet and Triplet Excited States.** With the prerequisite ground-state DFT calculation in hand, we proceed to the time-dependent calculation on  $[\text{RuL}'_2(\text{NCS})_2]^{4-}$  to find the characters and energies of its low-lying excited states. We begin with the singlet  $\rightarrow$  singlet spin-allowed transitions. The energy of each excited state is the vertical excitation energy in electron-volts (eV) from the ground state. Seventy such excited states had to be considered in order to encompass the 1.7 eV window of visible absorptions exhibited by this chromophore, a fact that testifies to the complexity of this molecule's excited-state electronic structure. The 21 transitions with the greatest oscillator strengths are listed in Table 2 (see Table S1 for all calculated singlet states); this information is also presented graphically for all calculated excited states in Figure 4a. There are excited states having significant oscillator strength throughout the 2–3.7 eV region, but the strongest are clustered around 2.4 and 3.2 eV (referred to as the first and second bands, respectively). While these transitions are reasonably strong, the largest calculated value of  $f$  is only 0.0748 (excited state 44). There are also three singlet excited states

**TABLE 1: Energies ( $E$ ) and Percent Compositions<sup>a</sup> of Frontier Molecular Orbitals Obtained from B3LYP/LanL2DZ Wavefunction for  $[\text{RuL}'_2(\text{NCS})_2]^{4-}$** 

MO <sup>b</sup>	144(O)	145(O)	146(O)	147(O)	148(O)	149(O)	150(O)	151(O)	152(O)	153(O)	154(V)	155(V)	156(V)	157(V)	
$E$ (eV)	2.533	2.549	2.579	2.841	2.919	3.003	3.016	3.048	3.077	3.285	6.021	6.179	6.600	6.859	
Ru(1)	0.1	0.0	1.0	1.0	4.5	14.8	6.2	19.0	45.0	51.0	4.5	5.9	2.2	2.7	
N(12)	0.0	0.0	0.2	0.7	0.0	0.1	0.1	0.2	0.1	0.2	1.2	6.3	7.5	1.7	
O(4)	0.0	0.1	0.0	45.9	0.0	0.1	0.1	0.0	0.7	1.2	0.0	0.1	1.0	0.3	
O(5)	0.0	0.1	0.0	33.7	0.0	0.0	0.1	0.0	0.7	0.8	0.1	0.4	0.4	0.1	
N(13)	0.0	0.0	0.0	0.0	0.0	0.2	0.2	0.2	0.4	0.1	1.5	16.2	0.3	0.1	
O(6)	0.1	47.8	0.0	0.0	0.2	9.4	10.1	24.7	0.5	0.0	0.1	1.5	0.0	0.0	
O(7)	0.1	47.2	0.0	0.0	0.1	8.2	8.7	21.6	0.3	0.1	0.0	0.6	0.2	0.0	
N(14)	0.2	0.0	0.2	0.0	0.0	0.1	0.1	0.1	0.3	0.3	9.7	1.6	0.5	1.4	
O(8)	55.6	0.1	1.9	0.0	0.3	19.1	37.3	1.2	4.1	0.5	0.2	0.0	0.1	0.0	
O(9)	36.3	0.1	0.9	0.0	0.0	4.4	9.3	0.3	1.4	0.0	0.7	0.1	0.0	0.2	
N(15)	0.0	0.0	0.0	0.0	0.2	0.1	0.1	0.1	0.9	0.2	12.4	1.1	1.3	9.4	
O(10)	0.4	0.0	0.1	0.0	25.8	3.5	0.3	1.3	0.2	0.0	1.1	0.1	0.1	1.0	
O(11)	0.4	0.0	0.0	0.0	42.7	5.2	0.5	1.9	0.2	0.0	0.5	0.0	0.3	2.5	
N(16)	0.6	0.0	11.5	0.4	0.4	1.0	0.1	0.1	7.9	4.8	0.1	0.2	0.1	0.1	
C(42)	0.4	0.0	0.0	0.0	0.0	0.0	0.0	0.0	0.0	0.0	0.0	0.0	0.0	0.0	
S(2)	1.6	0.0	28.0	1.0	1.0	2.3	0.1	0.2	19.4	11.7	0.1	0.1	0.0	0.0	
N(17)	0.1	0.0	11.8	0.2	1.3	2.5	1.3	3.3	0.7	3.7	0.4	0.0	0.1	0.0	
C(43)	0.0	0.3	0.0	0.0	0.0	0.0	0.0	0.0	0.0	0.0	0.0	0.0	0.0	0.0	
S(3)	0.4	0.1	42.4	0.7	4.4	8.7	4.3	11.4	2.3	12.6	0.0	0.1	0.1	0.0	
Type <sup>c</sup>	COO <sup>-</sup>	COO <sup>-</sup>	NCS	COO <sup>-</sup>	COO <sup>-</sup>	COO <sup>-</sup>	COO <sup>-</sup>	COO <sup>-</sup>	COO <sup>-</sup>	Ru(d*)	Ru(d*)	bpy( $\pi^*$ )	bpy( $\pi^*$ )	bpy( $\pi^*$ )	bpy( $\pi^*$ )

<sup>a</sup> Bipyridine carbons are not listed as their contributions are negligible for the occupied orbitals shown. <sup>b</sup> O: occupied; V: virtual. <sup>c</sup> Type: dominant moiety contributing to molecular orbital.

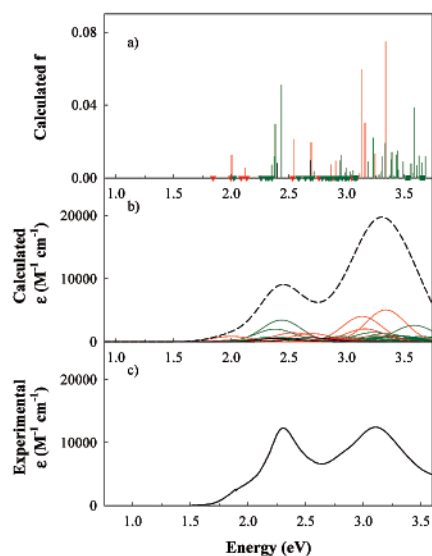


**Figure 4.** Calculated and experimental visible absorption spectra of  $[\text{RuL}'_2(\text{NCS})_2]^{4-}$ . (Note: the calculated plots have been shifted by 0.146 eV in this figure — see text for further details.) (a) Calculated oscillator strength,  $f$ , of singlet  $\rightarrow$  singlet and singlet  $\rightarrow$  triplet transitions. Red lines: singlet  $\rightarrow$  singlet MLCT transitions. Green lines: singlet  $\rightarrow$  singlet LBCT transitions. Black lines: singlet  $\rightarrow$  singlet mixed transitions. Green squares: singlet  $\rightarrow$  singlet LBCT transitions ( $f = 0$ ). Red triangles: singlet  $\rightarrow$  triplet MLCT transitions ( $f = 0$ ). Green triangles: singlet  $\rightarrow$  triplet LBCT transitions ( $f = 0$ ). (b) Calculated absorption spectrum based on the above transitions, assuming each transition is a Gaussian with a full width at half-maximum (fwhm) of 0.4 eV. Red curves: MLCT absorptions. Green curves: LBCT absorptions. Black curves: mixed character absorptions. Dashed curve: total absorption calculated as the sum of all of these transitions. (c) Experimental absorption spectrum of  $\text{Ru}(\text{H}_2\text{L}')_2(\text{NCS})_2$  obtained in ethanol solution.

with zero oscillator strength (green squares on the baseline of Figure 4a). These states, although present in the molecule's excited-state manifold, will therefore not contribute significantly to the compound's absorption cross-section. No excited states or absorption features were found below 1 eV.

A commonly used model of an excited state corresponds to excitation of an electron from an occupied to a virtual MO (i.e., a one-electron picture). However, the excited states calculated herein demonstrate that excited-state electronic structures are best described in terms of multielectronic states, wherein a linear combination of several occupied-to-virtual MO excitations comprises a given optical transition. For simplicity, Table 2 lists only the most significant contributions to each excited state. Where multiple excitations are of comparable importance (i.e., excitations with coefficients at least 85% of the dominant one; see Table S1), each is listed. Assignment of the character of each excited state was based on the compositions of the occupied and virtual MOs of the dominant excitation(s) for that excited state. For example, when the occupied orbital is metal-based and the virtual orbital is bipyridine  $\pi^*$ -based, the transition is designated a metal-to-ligand charge transfer (MLCT). Similarly, when the occupied orbital is localized on a ligated moiety and the virtual orbital type is bipyridine  $\pi^*$ , the transition is designated LBCT (ligand-based charge transfer, corresponding to either intra- or inter-ligand charge transfer). For the majority of the excited states calculated, such an assignment can be made unambiguously. However, excited states 7 and 10 exhibit comparable LBCT and MLCT contributions; we refer to these excited states as having mixed character. Figure 5 illustrates the difference between LBCT and MLCT excitations for two strongly allowed transitions. Figure 5a shows the dominant single-electron excitation of the most strongly allowed <sup>1</sup>LBCT transition (from MO 148 to MO 154), corresponding to excited state 8. This excitation is from a MO centered on one carboxylate group to a MO spanning a bipyridine moiety (though both MOs have noticeable contributions from ruthenium). Figure 5b shows the dominant single-electron excitation of the most strongly allowed <sup>1</sup>MLCT excitation (from MO 152 to MO 159), corresponding to excited state 44. Here, the excitation is from a ruthenium d orbital (which is interacting with one of the NCS groups) to a bipyridine-based  $\pi^*$  orbital.

Given that the HOMO of  $[\text{RuL}'_2(\text{NCS})_2]^{4-}$  ( $\sim 2.7$  eV below the bipyridine  $\pi^*$  LUMO) is mainly ruthenium d orbital in

**TABLE 2: Selected Calculated Excited States for  $[\text{RuL}'_2(\text{NCS})_2]^{4-}$ <sup>a</sup>**

State	$E$ (eV) <sup>b</sup>	$f$ <sup>c</sup>	$\phi_o \rightarrow \phi_v$ <sup>d</sup>	Character <sup>e</sup>
Singlet Excited States				
1	2.003	0.0125	153 $\rightarrow$ 154	MLCT
5	2.372	0.0116	150 $\rightarrow$ 154	LBCT
6	2.381	0.0295	149 $\rightarrow$ 154	LBCT
8	2.436	0.0510	148 $\rightarrow$ 154	LBCT
9	2.540	0.0210	152 $\rightarrow$ 155	MLCT
11	2.693	0.0194	153 $\rightarrow$ 156	MLCT
20	2.950	0.0123	144 $\rightarrow$ 154	LBCT
			146 $\rightarrow$ 154	
32	3.134	0.0595	153 $\rightarrow$ 158	MLCT
33	3.159	0.0301	153 $\rightarrow$ 159	MLCT
37	3.232	0.0219	137 $\rightarrow$ 154	LBCT
			151 $\rightarrow$ 157	
38	3.246	0.0132	152 $\rightarrow$ 158	MLCT
42	3.306	0.0118	142 $\rightarrow$ 155	LBCT
			142 $\rightarrow$ 154	
43	3.335	0.0191	149 $\rightarrow$ 158	LBCT
44	3.339	0.0748	152 $\rightarrow$ 159	MLCT
47	3.384	0.0100	143 $\rightarrow$ 155	LBCT
48	3.393	0.0141	143 $\rightarrow$ 155	LBCT
51	3.431	0.0127	149 $\rightarrow$ 159	LBCT
			151 $\rightarrow$ 159	
52	3.441	0.0148	137 $\rightarrow$ 155	LBCT
60	3.584	0.0386	135 $\rightarrow$ 154	LBCT
64	3.625	0.0121	136 $\rightarrow$ 155	LBCT
70	3.681	0.0119	143 $\rightarrow$ 156	LBCT
Triplet Excited States				
1	1.842	0.0000	153 $\rightarrow$ 154	MLCT
2	1.997	0.0000	153 $\rightarrow$ 155	MLCT
3	2.023	0.0000	151 $\rightarrow$ 154	LBCT
4	2.086	0.0000	152 $\rightarrow$ 155	MLCT
5	2.134	0.0000	152 $\rightarrow$ 154	MLCT
6	2.259	0.0000	151 $\rightarrow$ 155	LBCT
7	2.302	0.0000	148 $\rightarrow$ 154	LBCT
8	2.324	0.0000	150 $\rightarrow$ 154	LBCT

<sup>a</sup> See the Supporting Material for more complete listings. <sup>b</sup> Energy above the ground state (vertical excitation). <sup>c</sup> Oscillator strength. <sup>d</sup> Occupied ( $\phi_o$ ) to virtual ( $\phi_v$ ) orbital excitation. <sup>e</sup> Character of excited state: metal-to-ligand charge transfer (MLCT) or ligand-based charge transfer (LBCT, either intra- or inter-ligand charge transfer).

character, it is not surprising that the lowest-energy transitions are MLCT in nature. Similarly, ligand-based excited states contribute due to the presence of occupied carboxylate orbitals less than 3.2 eV below the LUMO and an isothiocyanate orbital less than 3.5 eV below the LUMO. On the other hand, no d–d transitions are observed within the first seventy excited states due to the relatively high energy of the lowest unoccupied ruthenium orbital (MO 162; 5.3 eV above the HOMO). This is consistent with the expectation that charge-transfer states are generally lower in energy than ligand-field bands for most second-row transition metal complexes. These factors should facilitate injection since the lowest-energy excited states are localized on bipyridine, which in turn is connected to the  $\text{TiO}_2$  via the anchoring carboxy group.

The frontier electronic structure (Figure 2) shows that there is a much greater density of occupied orbitals than virtual ones: there are nineteen occupied MOs (MOs 135–153) within 4.2 eV below the LUMO of  $[\text{RuL}'_2(\text{NCS})_2]^{4-}$  but only six virtual MOs (MOs 154–159) within 4.2 eV above the HOMO. Thus, as the transition energy increases, transitions tend to originate from lower occupied MOs rather than terminate in higher virtual MOs (see Table 2). This trend does not go so far, however, as to produce any  $\pi \rightarrow \pi^*$  states in the first seventy excited states due to the fact that the highest-energy occupied ligand  $\pi$  orbital, MO 134, is over 4.8 eV below the LUMO.

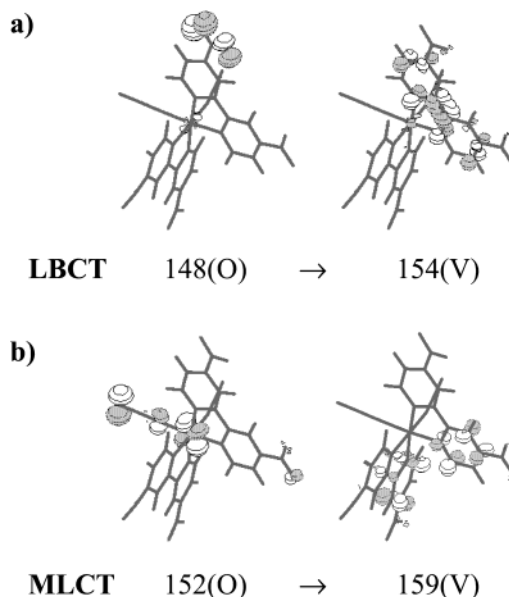


**Figure 5.** Example of dominant occupied and virtual orbitals for two different types of excitations. (a) Ligand-based charge transfer (LBCT) excitation from MO 148 to MO 154. (b) Metal-to-ligand charge transfer (MLCT) excitation from MO 152 to MO 159.

Examining the lower-energy MLCT transitions, we see that the virtual orbitals ( $\phi_v$ ) are either MO 154 or 155 for lower-energy excitations ( $E < 2.6$  eV), and MOs 156 or 157 for transitions energies in the range of 2.6–3 eV. This makes intuitive sense because the former MOs are delocalized over both halves of a bipyridine, while the latter two MOs are localized on one bipyridine moiety and thus higher in energy (Figure 3).

The 35 lowest-energy triplet excited states were also calculated, using analogous TD-DFT methodology. The first eight triplet excited states are listed in Table 2; all 35 states calculated are illustrated graphically in Figure 4a (and listed in Table S2). Both MLCT and LBCT excited states are seen, as with the singlets, because frontier occupied ruthenium-rich MOs, carboxylate-based MOs, and isothiocyanate-based MOs are relatively close in energy to virtual bipyridine-based  $\pi^*$  MOs. For the MLCT states, the energy ordering of the dominant occupied-to-virtual orbital excitations is roughly the same as that observed for the singlet manifold. As expected from Hund's rule, transitions to the triplet states tend to be lower in energy than their corresponding singlets. For example, the first triplet vertical transition energy is 0.161 eV lower than that of the first singlet excited state (1.842 vs 2.003 eV) where both represent (predominantly) a MO 153  $\rightarrow$  MO 154 (MLCT) transition. Because singlet  $\rightarrow$  triplet transitions are formally spin forbidden, all have zero oscillator strength since singlet–triplet mixing was not taken into account in these calculations. It is thus not possible from our results to determine what effect these triplet states have on the ground-state absorption spectrum of  $[\text{RuL}'_2(\text{NCS})_2]^{4-}$ . However, since the contribution from triplet excited states is quite small in the experimental spectrum, this should not cause major discrepancies between theory and experiment. Last, we point out that the energies of the triplet states quoted herein are of limited utility for assessing their thermodynamic relevance for injection. That is, due to their small radiative cross-sections, the dominant mechanism for their population is nonradiative relaxation from the singlets. The energies of these triplet states upon formation therefore may or may not be comparable to the vertical transition energies afforded by these calculations.

**Comparison with Experimental Results.** To independently check that these calculations produce reasonable results, the

absorption spectrum of  $[\text{RuL}'_2(\text{NCS})_2]^{4-}$  was simulated based on the TD-DFT calculations (Figure 4b). Here, each excited state having  $f > 0$  (i.e., each vertical line in Figure 4a) was modeled as a Gaussian feature. Selection of the full width at half-maximum (fwhm) of each Gaussian was based upon the spectral fitting performed by Yang et al. for the electronic absorption spectrum of  $\text{Na}_2[\text{Fe}(\text{bpy})(\text{CN})_4]$  in aqueous solution: these authors found the fwhm of the MLCT peak near 2.7 eV ( $20000\text{ cm}^{-1}$ ) to be  $\sim 0.41\text{ eV}$  ( $\sim 3300\text{ cm}^{-1}$ ).<sup>41</sup> For simplicity, we rounded this value to 0.4 eV and used the same fwhm for both LBCT and mixed-character excited states. The calculated oscillator strength  $f$  was related to the molar absorptivity  $\epsilon$  (in  $\text{M}^{-1}\text{ cm}^{-1}$ ) according to<sup>42</sup>

$$f = 4.315 \times 10^{-9} \int_{-\infty}^{\infty} \epsilon(\bar{\nu}) d\bar{\nu} \quad (1)$$

where  $\bar{\nu}$  is the transition energy in wavenumbers ( $\text{cm}^{-1}$ ).

The graph of calculated molar absorptivity as a function of energy (Figure 4b) shows a Gaussian corresponding to each of the 67 calculated singlet excited states with  $f > 0$ ; transitions to triplets are spin-forbidden and thus have  $f = 0$  (see above). The Gaussian curves are shaded based on whether they are primarily MLCT (red), LBCT (green), or mixed (black) in origin. The total absorption spectrum (dashed curve) is the sum of these Gaussians. It should be noted that the shape of the total absorption spectrum at the highest energies shown could be modified somewhat by excited states higher in energy than those we calculated.

The experimental molar absorptivity spectrum of  $\text{Ru}(\text{H}_2\text{L}')_2(\text{NCS})_2$  dissolved in ethanol is shown in Figure 4c. A spectrophotometric titration in ethanol, analogous to that of Nazeeruddin et al. in 5:1 water/ethanol,<sup>36</sup> verified that the predominant protonation state in ethanol is in fact  $[\text{RuL}'_2(\text{NCS})_2]^{4-}$ .<sup>43</sup> Before any comparisons are made, we note that  $[\text{RuL}'_2(\text{NCS})_2]^{4-}$  is effectively in the gas phase as far as the TD-DFT calculations are concerned. Though we have partially compensated for this by assigning spectral bandwidths appropriate for solution-phase absorption features in Figure 4b, other effects due to solvent (e.g., solvation energy) have not been accounted for. In addition, singlet-triplet mixing (facilitated by spin-orbit coupling), which would redistribute some intensity from singlet  $\rightarrow$  singlet to singlet  $\rightarrow$  triplet transitions, has not been taken into account in these calculations. Nevertheless, a comparison of the energy of the first intense peak revealed only a 0.146 eV difference between the calculated and experimental spectra; for ease of comparison, we have horizontally offset the calculated plots in Figure 4 by this amount so the first intense peaks line up on the page. This level of quantitative agreement is quite good given both the neglect of solvation energy and the tendency for the B3LYP functional to overestimate HOMO-LUMO gaps for transition metal complexes.<sup>44</sup> We note that the relative energy and molar absorptivity of the low-energy rising shoulder, the first band maximum, and the second band maximum given by our simulation are all in reasonable agreement with the experimental spectrum (at approximately 1.8, 2.4, and 3.2 eV, respectively). In addition, the energy spacing between the two band maxima differs by only 0.057 eV as compared to the experimental spectrum. We can compare our results with the semiempirical calculations of Rensmo et al. on the related complex  $\text{Ru}(\text{bpy})_2(\text{NCS})_2$ , for which the average error in the energy of the two peaks is  $\sim 0.21\text{ eV}$  and the interpeak spacing error is  $\sim 0.10\text{ eV}$  compared to their experimental spectrum in dimethylformamide.<sup>29</sup> The fact that the peak spacing for the TD-DFT-based method agrees with experiment relatively well,

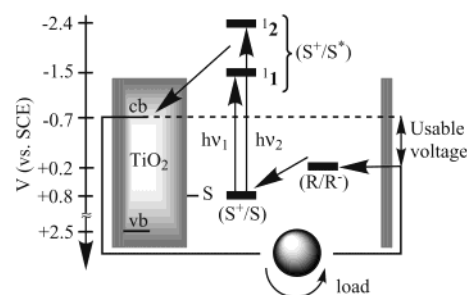


**Figure 6.** Schematic diagram of  $\text{Ru}(\text{H}_2\text{L}')_2(\text{NCS})_2/\text{TiO}_2$  solar cell showing the  $\text{TiO}_2$  valence band (vb) and conduction band (cb),  $\text{Ru}(\text{H}_2\text{L}')_2(\text{NCS})_2$  sensitizer (S), redox agent (R), and load. The sensitizer may be excited from its ground state ( $\text{S}^+/\text{S}$ ) to an excited state ( $\text{S}^+/\text{S}^*$ ); two are shown here, namely those represented by the first intense peak in the absorption spectrum ( $h\nu_1$ ,  $^1\text{S}^+/\text{S}^*$  state) and the second ( $h\nu_2$ ,  $^2\text{S}^+/\text{S}^*$  state). Other arrows show the path of a current-producing electron around the cell. The energy levels of the vb, cb, dye ground state, and  $\text{R}/\text{R}^-$  were taken from Kalyanasundaram and Grätzel;<sup>3</sup> the dye excited states are those calculated herein, corrected for the 0.146 eV offset between theoretical and experimental spectra (see text).

at least within the energy range studied, is encouraging because simply shifting all calculated energies by the same fixed offset (0.146 eV) yields good agreement with experiment.

The calculated molar absorptivity at any given wavelength is a function of the full width at half-maximum chosen for the Gaussians: a larger fwhm would spread each Gaussian out along the energy axis and tend to produce lower  $\epsilon$  values at the peaks but larger values elsewhere, while a smaller fwhm would yield more intense but narrower peaks for a transition of a given oscillator strength. Assuming that the fwhm values we have chosen are appropriate, the simulation slightly underestimates the molar absorptivity of the first band maximum and significantly overestimates that of the second band maximum. This is perhaps not surprising since, from a comparison between TD-DFT and the more expensive CASPT2 method, the results of Full et al. show that TD-DFT oscillator strengths diverge more from the CASPT2 values as excitation energy increases.<sup>45</sup> In addition, a similar comparison by Tozer et al. showed that TD-DFT has difficulty distributing intensity properly;<sup>46</sup> it is thus possible that intensity is erroneously shifted from the first band maximum to the second in our calculations. The rising shoulder ( $\sim 1.8\text{ eV}$ ) would probably be better reproduced if singlet  $\rightarrow$  triplet mixing were taken into account, since it is in this region where a transition to a  $^3\text{MLCT}$  state is expected.<sup>47</sup> Overall, though, the simulation reproduces the experimental spectrum quite well.

The good agreement between theory and experiment suggests that the character of the experimental absorption features may be inferred from our calculations. Specifically, the low-energy edge ( $\sim 1.8\text{ eV}$ ) is largely MLCT in nature, whereas the first ( $\sim 2.4\text{ eV}$ ) and second peaks ( $\sim 3.2\text{ eV}$ ) contain significant contributions from both LBCT and MLCT transitions; qualitatively similar results were reached in a previous study for a closely related complex.<sup>29</sup> Our results indicate that LBCT excited states contribute significantly to the visible absorption in addition to the MLCT states which are typically believed to dominate the spectrum. Thus, assignment of a broad band to a single type, as has traditionally been done in the literature by applying empirical rules to experimental data, appears overly simplified for the present complex.

**Molecular Engineering of a  $\text{Ru}(\text{H}_2\text{L}')_2(\text{NCS})_2$ -Sensitized Solar Cell.** We now turn to the issue of which excited states are likely to inject electrons into the conduction band of  $\text{TiO}_2$ . Using the potentials shown in Figure 6, the ground state of

$\text{Ru}(\text{H}_2\text{L}')_2(\text{NCS})_2$  is 1.5 V below the conduction band of  $\text{TiO}_2$ . We thus take 1.5 eV as roughly the energy an excited state must have (either thermalized or nonthermalized) to inject an electron into the semiconductor. We also make the approximation that the sensitizer's energetics are not too different whether it is in ethanol or adsorbed to  $\text{TiO}_2$ ; this appears reasonable given the agreement between the absorption spectra of  $\text{Ru}(\text{H}_2\text{L}')_2(\text{NCS})_2$  in ethanol solution and when bound to  $\text{TiO}_2$ .<sup>31</sup> Adjusting for the 0.146 eV offset between theoretical and experimental excitation energies determined for the first singlet absorption maxima (see above), an excited state should have a theoretical excitation energy of 1.646 eV to be able to inject. All the singlets calculated are thus sufficiently energetic, assuming injection takes place at or near the Franck–Condon region.<sup>48</sup> This kind of direct injection would constitute electron transfer from nonthermalized excited states, a process which has been observed for  $\text{Ru}(\text{H}_2\text{L}')_2(\text{NCS})_2$  bound to various semiconductors<sup>30,49,27</sup> and, by inference, for a related iron sensitizer into  $\text{TiO}_2$ .<sup>50</sup> All of the virtual orbitals involved are predominately bipyridine  $\pi^*$ , which should facilitate injection since the sensitizer is anchored to  $\text{TiO}_2$  via the dicarboxy-bipyridyl ligand.<sup>3</sup> However, not all singlet excited states contribute equally to the absorption cross-section of the chromophore. Excited states 8, 32, and 44 (at corrected energies of approximately 2.3, 3.0, and 3.2 eV, respectively) have the greatest oscillator strengths (0.0510, 0.0595, and 0.0748, respectively), as well as sufficient driving forces to inject (approximately 0.8, 1.5, and 1.7 eV, respectively). These are therefore likely candidates for efficient excited-state formation and subsequent injection. Other states appear less likely to play a role in injection immediately upon illumination: states 29, 56, and 66, for example, have zero oscillator strength and therefore are not directly populated upon irradiation. Ten other states calculated have oscillator strengths less than 0.0005, so they absorb  $\sim 100$  times fewer photons than the three strongest-absorbing states.

One question of interest is whether triplet excited states, being lower in energy than their singlet counterparts, have enough energy to inject electrons into the semiconductor. Unfortunately, our calculations cannot directly address this question since the triplets are predominately populated by nonradiative relaxation from singlets rather than by vertical excitation by a photon.

In Figure 6 we present a summary picture of the energetics of a  $\text{TiO}_2$ -based photoelectrochemical solar cell sensitized with  $\text{Ru}(\text{H}_2\text{L}')_2(\text{NCS})_2$ . Redox potentials for the valence band (vb, +2.5 V vs SCE), sensitizer ground state ( $\text{S}^+/\text{S}$ , +0.8 V), and conduction band (cb, -0.7 V) were taken from the literature.<sup>3</sup> The first two intense singlet  $\rightarrow$  singlet absorption peaks derived from our calculations have been included and are labeled **1** (-1.5 V) and **2** (-2.4 V). Triplet states were not considered because of their relatively minor contribution to the experimental absorption cross-section,<sup>47</sup> although they clearly play an important role in electron injection.<sup>27</sup> The calculated transition energy of each singlet was corrected to the experimental ethanolic solution value by subtracting 0.146 eV (see above). Although the pH difference between neat ethanol and the electrolytic solution of a functional cell may shift the absorption spectrum somewhat, this is a fairly minor effect ( $\sim 0.1$  V<sup>36</sup>). From a molecular engineering standpoint, excess photon energy producing excited state **2** is wasted in the injection step; ideally, a cell would extract more voltage from such ultraviolet photons.

## Conclusions

We have used DFT methods to study the ground and excited electronic structures of the common solar cell dye  $[\text{RuL}'_2-$

$(\text{NCS})_2]^{4-}$  in order to better understand what properties help make it an effective sensitizer in  $\text{TiO}_2$ -based photoelectrochemical cells. The electronic absorption spectrum calculated from time-dependent density functional theory was in good agreement with the experimental molar absorptivity spectrum in ethanol, with only a 0.146 eV difference in the first absorption maxima. More significantly, the relative energies of the two main peaks were well reproduced, and their molar absorptivities were in reasonable agreement. The following features of this compound are likely important in making it a good sensitizer:

(1) Low-lying occupied carboxylate-based MOs are energetically similar to the  $\text{TiO}_2$  valence band which could facilitate adsorption;

(2) The lowest eight unoccupied MOs are bipyridine  $\pi^*$  in character, from which injection into the  $\text{TiO}_2$  conduction band is expected to be likely given their spatial proximity. The TD-DFT calculations of 70 singlets and 35 triplets found both MLCT and LBCT excited states, but no states of d–d character. Thus, all of these calculated excited states are associated with bipyridine( $\pi^*$ ) virtual orbital(s) and are therefore reasonable candidates for effecting electron injection. The density of excited electronic states is quite high (70 singlets within a 1.7 eV window), suggesting that rather than viewing the excited levels as different vibrational quanta within the same electronic state, the absorption manifold be viewed to a reasonable approximation as a multitude of closely spaced electronic states;

(3) All of the singlet excited states calculated have sufficient energy for injection at or near the Franck–Condon region. On the basis of three calculated properties of these excited states—energy, oscillator strength, and spatial localization on anchoring ligands—the most efficient excited-state formation and subsequent electronic injection is expected at excitation energies of approximately 2.3, 3.0, and 3.2 eV. A number of triplet states were also identified. However, they are populated largely through nonradiative processes which our calculations do not address.

To improve the efficiency of a molecular device such as a dye-sensitized solar cell, molecular engineering strategies can be employed to manipulate the energetics of the sensitizer. Clearly, it is important in this context to understand in detail the sensitizer's electronic structure. Our results suggest that DFT-based methods can play a significant role in this endeavor.

**Acknowledgment.** We thank Dr. V. Shklover and Yu. Ovchinnikov for providing their X-ray geometry for  $\text{Ru}(\text{H}_2\text{L}')_2(\text{NCS})_2$  in Cartesian coordinates. We gratefully acknowledge financial support from the Petroleum Research Fund administered by the American Chemical Society (Grant 36108-AC6), the Center for Fundamental Materials Research at Michigan State University, the Alfred P. Sloan Foundation, and the Chemical Sciences, Geosciences and Biosciences Division, Office of Basic Energy Sciences, Office of Science, U.S. Department of Energy (Grant DE-FG02-01ER15282) (J.K.M.). In addition, computer allocation grants provided by the National Center for Supercomputer Applications (NCSA) and Michigan State University (NSF Grant CHE 9974834) are gratefully acknowledged.

**Supporting Information Available:** Tables listing all 70 singlet excited states and all 35 triplet excited states calculated. This material is available free of charge via the Internet at <http://pubs.acs.org>.

## References and Notes

- (1) O'Regan, B.; Grätzel, M. *Nature* **1991**, *353*, 737.

- (2) Nazeeruddin, M. K.; Kay, A.; Rodicio, I.; Humphrybaker, R.; Müller, E.; Liska, P.; Vlachopoulos, N.; Grätzel, M. *J. Am. Chem. Soc.* **1993**, *115*, 6382.
- (3) Kalyanasundaram, K.; Grätzel, M. *Coord. Chem. Rev.* **1998**, *177*, 347.
- (4) Moser, J. E.; Bonnôte, P.; Grätzel, M. *Coord. Chem. Rev.* **1998**, *171*, 245.
- (5) Hagfeldt, A.; Grätzel, M. *Acc. Chem. Res.* **2000**, *33*, 269.
- (6) Heimer, T. A.; D'Arcangelis, S. T.; Farzad, F.; Stipkala, J. M.; Meyer, G. J. *Inorg. Chem.* **1996**, *35*, 5319.
- (7) Hannappel, T.; Burfeindt, B.; Storck, W.; Willig, F. *J. Phys. Chem. B* **1997**, *101*, 6799.
- (8) Tachibana, Y.; Moser, J. E.; Grätzel, M.; Klug, D. R.; Durrant, J. R. *J. Phys. Chem.* **1996**, *100*, 20056.
- (9) Ellingson, R. J.; Asbury, J. B.; Ferrere, S.; Ghosh, H. N.; Sprague, J. R.; Lian, T. Q.; Nozik, A. J. *J. Phys. Chem. B* **1998**, *102*, 6455.
- (10) Kallioinen, J.; Lehtovuori, V.; Myllyperkiö, P.; Korppi-Tommola, J. *Chem. Phys. Lett.* **2001**, *340*, 217.
- (11) Waterland, M. R.; Kelley, D. F. *J. Phys. Chem. A* **2001**, *105*, 4019.
- (12) Moser, J. E.; Noukakis, D.; Bach, U.; Tachibana, Y.; Klug, D. R.; Durrant, J. R.; Humphry-Baker, R.; Grätzel, M. *J. Phys. Chem. B* **1998**, *102*, 3649.
- (13) Durrant, J. R.; Tachibana, Y.; Mercer, I.; Moser, J. E.; Grätzel, M.; Klug, D. R. *Z. Phys. Chem. (Muenchen)* **1999**, *212*, 93.
- (14) Asbury, J. B.; Wang, Y. Q.; Lian, T. Q. *J. Phys. Chem. B* **1999**, *103*, 6643.
- (15) Ellingson, R. J.; Asbury, J. B.; Ferrere, S.; Ghosh, H. N.; Sprague, J. R.; Lian, T.; Nozik, A. J. *Z. Phys. Chemie—Int. J. Res. Phys. Chem. Chem. Phys.* **1999**, *212*, 77.
- (16) Tachibana, Y.; Haque, S. A.; Mercer, I. P.; Durrant, J. R.; Klug, D. R. *J. Phys. Chem. B* **2000**, *104*, 1198.
- (17) Heimer, T. A.; Heilweil, E. J.; Bignozzi, C. A.; Meyer, G. J. *J. Phys. Chem. A* **2000**, *104*, 4256.
- (18) Asbury, J. B.; Hao, E. C.; Wang, Y. Q.; Lian, T. Q. *J. Phys. Chem. B* **2000**, *104*, 11957.
- (19) Wang, Y. Q.; Asbury, J. B.; Lian, T. Q. *J. Phys. Chem. A* **2000**, *104*, 4291.
- (20) Rehm, J. M.; McLendon, G. L.; Nagasawa, Y.; Yoshihara, K.; Moser, J.; Grätzel, M. *J. Phys. Chem.* **1996**, *100*, 9577.
- (21) Burfeindt, B.; Hannappel, T.; Storck, W.; Willig, F. *J. Phys. Chem.* **1996**, *100*, 16463.
- (22) Ghosh, H. N.; Asbury, J. B.; Weng, Y. X.; Lian, T. Q. *J. Phys. Chem. B* **1998**, *102*, 10208.
- (23) Ghosh, H. N.; Asbury, J. B.; Lian, T. Q. *J. Phys. Chem. B* **1998**, *102*, 6482.
- (24) Burfeindt, B.; Zimmermann, C.; Ramakrishna, S.; Hannappel, T.; Meissner, B.; Storck, W.; Willig, F. *Z. Phys. Chemie—Int. J. Res. Phys. Chem. Chem. Phys.* **1999**, *212*, 67.
- (25) Iwai, S.; Hara, K.; Murata, S.; Katoh, R.; Sugihara, H.; Arakawa, H. *J. Chem. Phys.* **2000**, *113*, 3366.
- (26) Willig, F.; Zimmermann, C.; Ramakrishna, S.; Storck, W. *Electrochim. Acta* **2000**, *45*, 4565.
- (27) Benkő, G.; Kallioinen, J.; Korppi-Tommola, J. E. I.; Yartsev, A. P.; Sundström, V. *J. Am. Chem. Soc.* **2002**, *124*, 489.
- (28) Rensmo, H.; Sodergren, S.; Patthey, L.; Westermark, K.; Vayssieres, L.; Kohle, O.; Bruhwiler, P. A.; Hagfeldt, A.; Siegbahn, H. *Chem. Phys. Lett.* **1997**, *274*, 51.
- (29) Rensmo, H.; Lunell, S.; Siegbahn, H. *J. Photochem. Photobiol. A—Chem.* **1998**, *114*, 117.
- (30) Moser, J. E.; Wolf, M.; Lenzenmann, F.; Grätzel, M. *Z. Phys. Chem. (Muenchen)* **1999**, *212*, 85.
- (31) Kuciauskas, D.; Monat, J. E.; Villahermosa, R.; Gray, H. B.; Lewis, N. S.; McCusker, J. K. *J. Phys. Chem. B*, in press.
- (32) Liu, D.; Kamat, P. V.; Thomas, K. G.; Thomas, K. J.; Das, S.; George, M. V. *J. Chem. Phys.* **1997**, *106*, 6404.
- (33) Barazzouk, S.; Lee, H.; Hotchandani, S.; Kamat, P. V. *J. Phys. Chem. B* **2000**, *104*, 3616.
- (34) Bickelhaupt, F. M.; Baerends, E. J. Kohn—Sham Density Functional Theory: Predicting and Understanding Chemistry. In *Reviews in Computational Chemistry*; Lipkowitz, K. B., Boyd, D. B., Eds.; Wiley-VCH: New York, 2000; Vol. 15, pp 1–86.
- (35) Shklover, V.; Ovchinnikov, Y. E.; Braginsky, L. S.; Zakeeruddin, S. M.; Grätzel, M. *Chem. Mater.* **1998**, *10*, 2533.
- (36) Nazeeruddin, M. K.; Zakeeruddin, S. M.; Humphry-Baker, R.; Jirousek, M.; Liska, P.; Vlachopoulos, N.; Shklover, V.; Fischer, C. H.; Grätzel, M. *Inorg. Chem.* **1999**, *38*, 6298.
- (37) Frisch, M. J.; Trucks, G. W.; Schlegel, H. B.; Scuseria, G. E.; Robb, M. A.; Cheeseman, J. R.; Zakrzewski, V. G.; Montgomery, J. A., Jr.; Stratmann, R. E.; Burant, J. C.; Dapprich, S.; Millam, J. M.; Daniels, A. D.; Kudin, K. N.; Strain, M. C.; Farkas, O.; Tomasi, J.; Barone, V.; Cossi, M.; Cammi, R.; Mennucci, B.; Pomelli, C.; Adamo, C.; Clifford, S.; Ochterski, J.; Petersson, G. A.; Ayala, P. Y.; Cui, Q.; Morokuma, K.; Malick, D. K.; Rabuck, A. D.; Raghavachari, K.; Foresman, J. B.; Cioslowski, J.; Ortiz, J. V.; Stefanov, B. B.; Liu, G.; Liashenko, A.; Piskorz, P.; Komaromi, I.; Gomperts, R.; Martin, R. L.; Fox, D. J.; Keith, T.; Al-Laham, M. A.; Peng, C. Y.; Nanayakkara, A.; Gonzalez, C.; Challacombe, M.; Gill, P. M. W.; Johnson, B. G.; Chen, W.; Wong, M. W.; Andres, J. L.; Head-Gordon, M.; Replogle, E. S.; Pople, J. A. *Gaussian 98*, revision A.9; Gaussian, Inc.: Pittsburgh, PA, 1998.
- (38) Zheng, K. C.; Wang, J. P.; Peng, W. L.; Liu, X. W.; Yun, F. C. *J. Phys. Chem. A* **2001**, *105*, 10899.
- (39) Rodriguez, J. H.; Wheeler, D. E.; McCusker, J. K. *J. Am. Chem. Soc.* **1998**, *120*, 12051.
- (40) Daul, C.; Baerends, E. J.; Vernooijs, P. *Inorg. Chem.* **1994**, *33*, 3538.
- (41) Yang, M.; Thompson, D. W.; Meyer, G. J. *Inorg. Chem.* **2000**, *39*, 3738.
- (42) Drago, R. S. *Physical Methods for Chemists*, 2nd ed.; Saunders College Publishing: Ft. Worth, 1992.
- (43) Monat, J. E.; McCusker, J. K. Unpublished results. The  $pK_a$  values were approximately 1.6 and 4.4 in ethanol.
- (44) Rodriguez, J. H.; Monat, J. E.; McCusker, J. K. Unpublished results.
- (45) Full, J.; Gonzalez, L.; Daniel, C. *J. Phys. Chem. A* **2001**, *105*, 184.
- (46) Tozer, D. J.; Amos, R. D.; Handy, N. C.; Roos, B. O.; Serrano-Andres, L. *Mol. Phys.* **1999**, *97*, 859.
- (47) Kalyanasundaram, K. *Photochemistry of Polypyridine and Porphyrin Complexes*; Academic Press: London, 1992.
- (48) Thermalization within the singlet state(s) prior to injection would require that the zero-point energy of the singlet lie above the conduction band edge. However, the present calculations do not provide information about this reorganization energy.
- (49) Moser, J. E.; Grätzel, M. *Chimia* **1998**, *52*, 160.
- (50) Ferrere, S.; Gregg, B. A. *J. Am. Chem. Soc.* **1998**, *120*, 843.